Crystal Structure of ATP Sulfurylase from *Penicillium chrysogenum*: Insights into the Allosteric Regulation of Sulfate Assimilation[†,‡]

Ian J. MacRae,[§] Irwin H. Segel,[§] and Andrew J. Fisher*[,§,||]

Section of Molecular and Cellular Biology and Department of Chemistry, University of California, One Shields Avenue, Davis, California 95616

Received February 21, 2001; Revised Manuscript Received April 11, 2001

ABSTRACT: ATP sulfurylase from *Penicillium chrysogenum* is an allosterically regulated enzyme composed of six identical 63.7 kDa subunits (573 residues). The C-terminal allosteric domain of each subunit is homologous to APS kinase. In the presence of APS, the enzyme crystallized in the orthorhombic space group (*I*222) with unit cell parameters of $a = 135.7$ Å, $b = 162.1$ Å, and $c = 273.0$ Å. The X-ray structure at 2.8 Å resolution established that the hexameric enzyme is a dimer of triads in the shape of an oblate ellipsoid 140 Å diameter × 70 Å. Each subunit is divided into a discreet N-terminal domain, a central catalytic domain, and a C-terminal allosteric domain. Two molecules of APS bound per subunit clearly identify the catalytic and allosteric domains. The sequence ^{197}QXRN^{200} is largely responsible for anchoring the phosphosulfate group of APS at the active site of the catalytic domain. The specificity of the catalytic site for adenine nucleotides is established by specific hydrogen bonds to the protein main chain. APS was bound to the allosteric site through sequence-specific interactions with amino acid side chains that are conserved in true APS kinase. Within a given triad, the allosteric domain of one subunit interacts with the catalytic domain of another. There are also allosteric−allosteric, allosteric−N-terminal, and catalytic−catalytic domain interactions across the triad interface. The overall interactions—each subunit with four others—provide stability to the hexamer as well as a way to propagate a concerted allosteric transition. The structure presented here is believed to be the R state. A solvent channel, 15−70 Å wide exists along the 3-fold axis, but substrates have access to the catalytic site only from the external medium. On the other hand, a surface "trench" links each catalytic site in one triad with an allosteric site in the other triad. This trench may be a vestigial feature of a bifunctional ("PAPS synthetase") ancestor of fungal ATP sulfurylase.

ATP sulfurylase and APS[1] kinase catalyze the first two steps in the assimilation of inorganic sulfate by a wide variety of organisms:

$$\mathrm{MgATP} + \mathrm{SO_4^{2-}} \rightleftharpoons \mathrm{MgPP_i} + \mathrm{APS}\ \text{(ATP sulfurylase)}$$

$$\mathrm{MgATP} + \mathrm{APS} \rightleftharpoons \mathrm{PAPS} + \mathrm{MgADP}\ \text{(APS kinase)}$$

PAPS, the product of the two-step sulfate activation sequence, serves as the sulfuryl donor for the biosynthesis of sulfate esters. The role of PAPS in sulfate ester formation is analogous to that of ATP in phosphate ester biosynthesis. In fungi, yeast, and most bacteria, PAPS is also the substrate for an NADPH-dependent reduction that yields sulfite. Sulfite is further reduced and then condensed with O-acetylserine to produce cysteine. APS rather than PAPS serves as the substrate for assimilatory sulfate reduction in higher plants and algae, and some bacteria. Together, the "activated sulfates" APS and PAPS, are the first products of a branched biosynthetic pathway leading to the production of all sulfur-containing biological molecules.

ATP sulfurylase from *Penicillium chrysogenum* is an oligomer composed of six identical 63.7 kDa subunits (573 residues). Unlike the enzyme from yeast, plants, and animals, the fungal enzyme is subject to allosteric inhibition by PAPS (*1*, *2*), the product of the APS kinase-catalyzed reaction. In the presence of PAPS, velocity curves (which are normally hyperbolic at pH 8 and 30 °C) become sigmoidal. The amino acid sequence of fungal ATP sulfurylase strongly suggests that the allosteric site is located in a C-terminal region, which appears to have been recruited from APS kinase (*3*). The C-terminal region also harbors the location of "SH-1" (Cys 509), a reactive sulfhydryl, which, if covalently modified (*4*) or replaced by Tyr or Ser (*5*), induces positive cooperativity in the absence of PAPS. Although the allosteric region

[†] The research described in this report was supported by NSF Grant MCB-9904003 to I.H.S. and A.J.F. and by the W. M. Keck Foundation Center for Structural Biology at the University of California, Davis. I.J.M. is supported from the Public Health Service/NIH training grant T32GM07377.

[‡] Protein coordinates have been deposited in the Protein Data Bank (filename 1I2D).

* To whom correspondence should be addressed. E-mail: fisher@chem.ucdavis.edu. Phone: (530) 754-6180. Fax: (530) 752-8995.

[§] Section of Molecular and Cellular Biology.

[||] Department of Chemistry.

[1] Abbreviations: APS, adenosine 5′-phosphosulfate (adenylyl sulfate); PAPS, 3′-phosphoadenosine 5′-phosphosulfate (adenylyl sulfate 3′-phosphate); MgATP, $MgPP_i$, MgADP, magnesium complexes of the corresponding substrates or products; Tris, tris-hydroxymethylaminomethane; EDTA, ethylenediamine tetraacetate; NEM, *N*-ethylmaleimide; DTNB, 5, 5′-dithiobis-(2-nitrobenzoate); MAD, multiple wavelength anomalous dispersion; SIR, single isomorphous replacement; rms, root-mean-square.

10.1021/bi010367w CCC: $20.00
Published on Web 05/17/2001

is about 40% identical in sequence to the core of true APS kinase and displays considerable structural homology (*6*), it does not possess measurable kinase activity (*5*). The absence of activity may be a result of the drastic modifications in the region of the P-loop and the substitution of Leu for the MgATP-interacting Asp at position 61 (*7*).

We previously determined the structure of the second enzyme of the sulfate activation pathway, APS kinase, from *P. chrysogenum* (*6*). The objective of the present study was to determine the structure of the first enzyme, ATP sulfurylase, from the same organism in order to locate the active site region, determine the functions of highly conserved residues, and to gain some insight into the physical nature of the allosteric transition.

EXPERIMENTAL PROCEDURES

Enzyme Assays. ATP sulfurylase activity in crude extracts was measured by the continuous spectrophotometric assay of the reverse (ATP synthesis) reaction. The reaction mixture contained 15 μM APS, 1 mM PP_i, 5 mM $MgCl_2$, 1 mM glucose, 0.6 mM $NADP^+$, and 2.5−5 units/mL each of sulfate-free hexokinase and G-6-P dehydrogenase all in 0.05 M Tris-Cl, pH 8.0 at 30 °C (*8*). During purification, the enzyme was assayed by the above method or by the continuous spectrophotometric molybdolysis assay, which measures the rate of AMP production. The latter reaction mixture contained 5 mM MgATP, 5 mM MoO_4^{2-}, 5 mM excess $MgCl_2$, 7 mM KCl, 0.4 mM PEP, 0.3 mM NADH, 2.5 units/mL of inorganic pyrophosphatase, 30 units/mL of adenylate kinase, 40 units/mL of pyruvate kinase, and 60 units/mL of lactate dehydrogenase (*1*).

Protein Expression and Purification. Native *P. chrysogenum* ATP sulfurylase was expressed in an *Escherichia coli* pET vector expression system (Novagen, Madison, WI) grown in LB media as described previously (*5*). A selenomethionine protein was produced by growing the same bacterial cell line in a modified M9 minimal media and introducing Se-met and methionine biosynthesis-inhibiting amino acids 20 min prior to induction of protein expression. Both the native and Se-met proteins were purified by Blue Dextran and DEAE cellulose column chromatography as described previously (*5*). After purification, the enzyme was dialyzed extensively against 10 mM Tris Cl, pH 8.0 plus 0.2 mM EDTA and then concentrated by membrane filtration to 10 mg of protein/mL. Crystals were grown by hanging drop vapor diffusion at 4 °C in 1.0 M sodium citrate, 2−4% ethylene glycol, 5 mM APS, and 100 mM Tris Cl, pH 8.0. APS was required for crystallization in this medium. Crystals of the space group *I*222 appeared after 2 weeks and typically grew to dimensions of 1.0 mm × 0.5 mm × 0.1 mm. These crystals had a V_M coefficient of 3.91 Å^3/Da (assuming three copies in the asymmetric unit), a solvent content of 69%, and the following unit cell parameters: $a = 135.67$ Å, $b = 162.09$ Å, $c = 273.00$ Å. Crystals were transferred to a cryoprotectant solution containing 1.1 M sodium citrate, 7% ethylene glycol, 5 mM APS, and 100 mM Tris Cl, pH 8.0 at 4 °C for several hours prior to being plunged into liquid nitrogen for transport out of the cold room. Although crystals of considerable size were easily obtained most were highly mosaic, many were twinned, and few diffracted X-rays beyond 5 Å resolution. However, after screening several dozen crystals a few were found to be of acceptable diffraction quality.

Data Collection and Phase Determination. The structure of ATP sulfurylase was determined by a combination of MAD and SIR methods. A 3.2 Å resolution MAD data set was collected at three wavelengths from a Se-met crystal on beamline 9-2 at the Stanford Synchrotron Radiation Laboratory (SSRL). Because of the large number of selenium sites (27 sites in the asymmetric unit) and the marginal quality of the data, we were unable to locate the position of any of the selenium atoms. A mercury derivative was produced by soaking a native crystal in cryoprotectant containing 1 mM thimersol for 24 h prior to cryo-cooling. A 2.8 Å data set was collected from this crystal on beamline 7-1 at the SSRL. All collected data were processed with DENZO and SCALEPACK (*9*). Three mercury sites were located in the thimersol data set by inspection of difference Patterson maps generated by the program PHASES (*10*) using the Se-met remote wavelength data as a "native." By entering these sites into a SOLVE (*11*) job, which combined the thimersol data set with the Se-met MAD data, we were able to locate all 27 selenium sites in the asymmetric unit. This produced phase estimates with an average figure of merit of 0.549 for all data from 50 to 3.2 Å resolution. Solvent flattening using RESOLVE (*12*, *13*) increased the figure of merit to 0.718. The initial solvent-flattened map clearly contained a noncrystallographic 3-fold. DM in the CCP4 program suite (*14*) was used to perform 3-fold averaging and phase extension to 2.8 Å resolution using amplitudes from the thimersol data set. Table 1 lists data collection and processing statistics.

Model Building and Refinement. The quality of the thimersol derivative data set was superior to that of any other data set collected and thus was used to build and refine the ATP sulfurylase model. The averaged and phase extended electron density map was used to build an initial model of a single ATP sulfurylase subunit with the molecular graphics program *O* (*15*). Noncrystallographic symmetry operators were used to generate the two other subunits in the asymmetric unit. Once all of the clear density had been modeled energy minimization and individual *B*-factor refinement were preformed with the program CNS (*16*). The noncrystallographic symmetry was tightly constrained throughout refinement for all atoms except residues 346−354, which form a surface loop that is slightly but clearly in different conformations in the three subunits. After multiple rounds of model building and refinement the conventional *R*-factor fell to 20.8% and the corresponding *R*-free (*17*) was 24.6%. A total of 87.2% of the residues fall within the most favored region of a Ramachandran plot, and none of the residues were in the disallowed region as determined by the program PROCHECK (*18*).

RESULTS

Crystallographic Properties. Crystals contained one ATP sulfurylase triad in the asymmetric unit with the three polypeptide chains designated as A, B, and C. The triad sat adjacent to a crystallographic 2-fold axis, which generated a hexamer with *D*3 symmetry. Subunit A was the best defined and had the lowest overall *B*-factor. In contrast, subunit C had an average *B*-factor of 91 Å^2 and many regions

Table 1: Data Collection, Phasing, and Refinement Statistics

	Thimersol	Se-met (peak)	Se-met (inflection)	Se-met (remote)
wavelength (Å)	1.08	0.979 05	0.979 27	0.956 67
resolution (Å)	2.8	3.2	3.2	3.2
no. of reflections ($I/\sigma > -2$)	257 680	213 675	214 070	212 366
no. of unique reflections	75 367	47 872	47 929	47 819
completeness (%)	95.9	97.7	97.8	97.6
R_{merge}[a] (%)	6.4	9.7	9.2	9.9
no. of sites (ASU)	3	27	27	27
figure of merit	0.549			

refinement statistics	
resolution (Å)	30.0−2.8
no. of reflections ($F > 0$)	75 367
R-factor[b]	20.7
R_{free}[b]	24.5
rms for bond distances (Å)	0.016
rms for bond angles (deg)	1.88
no. of non-hydrogen protein atoms	13 515
no. of water molecules	280
no. of APS atoms	162

[a] $R_{merge} = [\sum_h \sum_i |I_h - I_{hi}| / \sum_h \sum_i I_{hi}] \times 100$ where I_h is the mean of I_{hi} observations of reflection h. [b] R-factor and $R_{free} = \sum||F_{obs}| - |F_{calc}|| / \sum|F_{obs}| \times 100$ for 95% of recorded data (R-factor) or 5% of data (R_{free}).

of poorly defined electron density (the Wilson plot average temperature factor was 75.0 Å^2). This may be attributed to the fact that subunit C is involved in no crystal lattice contacts. Due to the quality and resolution of the data all three copies in the asymmetric unit were tightly restrained to their noncrystallographic 3-fold axis resulting in an average positional rms deviation of only 0.084 Å for all C-α atoms. Attempts to relax this restraint increased the R_{free} value. *B*-Factor refinement was not held to the same noncrystallographic symmetry constraints. Thimersol was found bound to Cys 42 in all three copies in the asymmetric unit. However, only the mercury atom of the thimersol modifier could be modeled with confidence. Cys 509, or "SH-1", was buried in a small hydrophobic pocket and was not modified by thimersol. All of the main chain atoms in residues 2−573 were clearly defined in subunits A and B. The following side chains were disordered and thus truncated to alanine in the final model: Asp 70, Lys 129, Lys 302, Glu 304, Lys 320, Glu 449, Lys 527, Glu 540, Lys 541.

Subunit Structure. Figure 1A shows the polypeptide chain of the *P. chrysogenum* ATP sulfurylase subunit. The subunit is divided into three distinct domains. The first 170 amino acid residues form an N-terminal domain comprised of a central antiparallel β sheet that is twisted into a partial β barrel and surrounded by α helices. Probing a three-dimensional database with the Cα backbone of this domain revealed no closely related structural homologues (*19*). Although it contains several patches of residues highly conserved among ATP sulfurylases from a variety of sources (50−64, 75−76, and 80−92 in the *P. chrysogenum* sequence) the N-terminal domain does not appear to be involved directly in catalysis.

The second domain (residues 171−395) packs tightly against the N-terminal region and contains the catalytic site. This catalytic domain adopts a dinucleotide-binding or Rossmann fold classically seen in dehydrogenases (*20*), but also observed in other adenylyl transferases (*21*, *22*). All of the amino acid residues that have been previously implicated in substrate binding and catalysis in ATP sulfurylase (*23*, *24*) are contained within this domain and a single APS molecule was bound near the top of its β sheet.

The third domain, composed of residues 396−573, is separate from the other two, connected by a short linker. This region, which has high sequence homology to APS kinase, adopts an α/β fold similar to that of true APS kinase (*6*), and almost certainly provides the allosteric PAPS binding site. The allosteric site may have a preference for PAPS (*1*), but at the exceedingly high APS concentrations required for crystallization (5 mM) it is not surprising to find APS bound there. Sequence 513−533, which corresponds to a disordered region in true APS kinase (residues 149−169) (*6*), is modeled clearly in the homologous allosteric domain of ATP sulfurylase.

Quaternary Structure. The hexamer is a dimer of triads (*D*3 symmetry) with one triad in the crystallographic asymmetric unit (Figure 1B). Subunits within a triad are arranged in a head to tail fashion with the catalytic domain of one subunit contacting the allosteric domain of the next. The triad lies adjacent to a crystallographic 2-fold that generates the complete hexamer. The hexameric enzyme is disk-shaped, i.e., has the form of an oblate ellipsoid with a diameter of 140 Å and a thickness of 70 Å (Figure 2).

The crystallographic 2-fold axis creates two types of "dimers" at the triad interface. These are termed the "allosteric domain dimer" (Figure 3A) and the "catalytic domain dimer" (Figure 3B). The allosteric domain dimer interface is similar to that observed in true APS kinase (*6*) but the two domains are rotated by about 35 degrees relative to each other. A salt link (between Arg 457 and Glu 443) and the packing of five hydrophobic residues stabilize the interface between allosteric domains. The hydrophobic residues are Leu 440, Val 461, Leu 465, Leu 431, and Phe 460, of which, the first three are present at the analogous subunit interface positions in true APS kinase. The salt link partners are also present in true APS kinase, but in that enzyme, they form an intrasubunit linkage. An allosteric domain also makes contacts with the N-terminal domain of one subunit and the catalytic domain of another subunit in the opposing triad. Of particular interest is a salt linkage between Arg 515 of the allosteric domain and Asp 111 of an adjacent N-terminal domain. This linkage may play a role in the allosteric transition (see below). Allosteric domain−

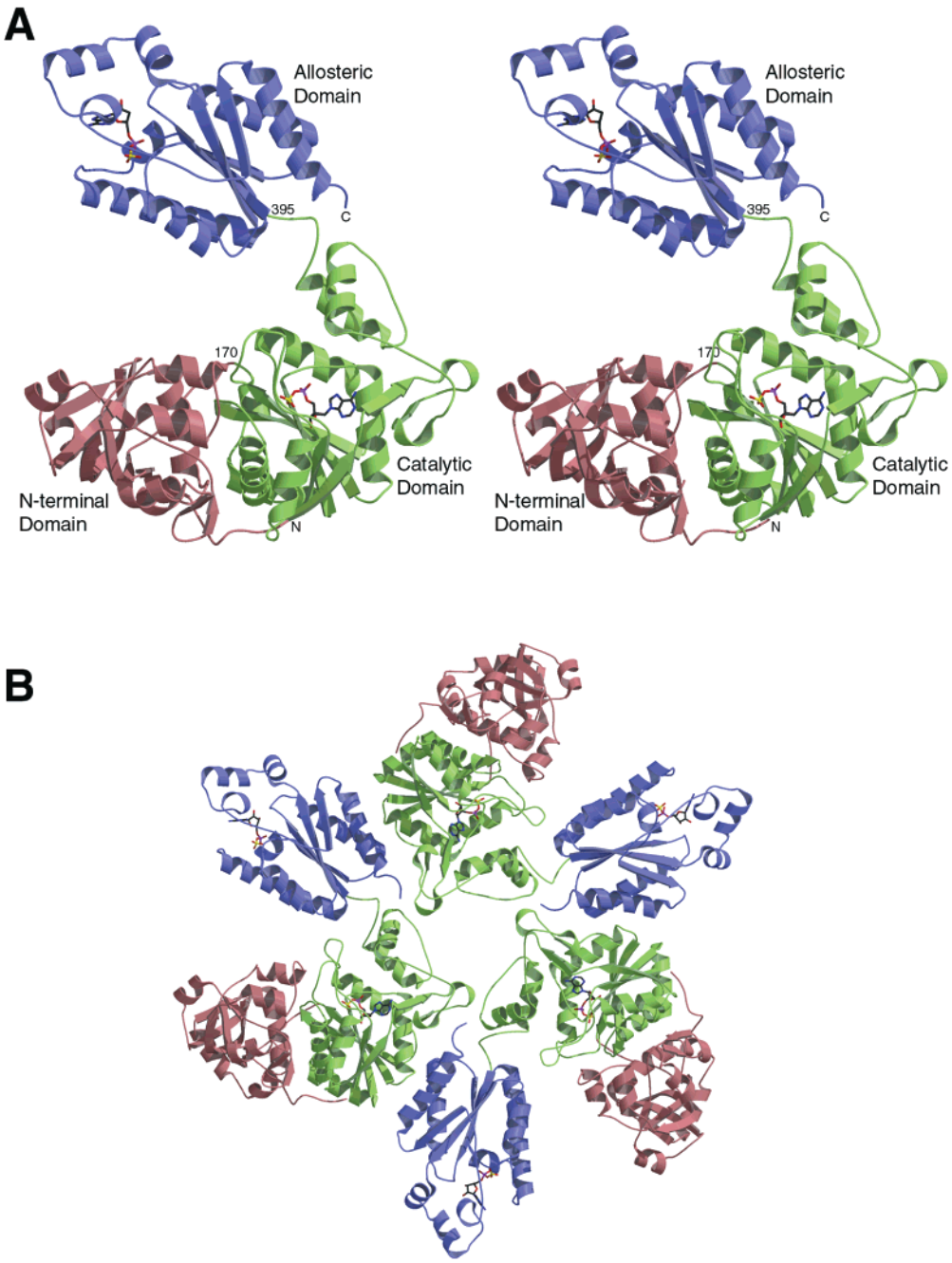

FIGURE 1: (A) Ribbon diagram (stereoview) of the *P. chrysogenum* ATP sulfurylase subunit (monomer). The subunit is divided into three distinct domains: N-terminal (salmon), catalytic (green), and allosteric (blue). (B) The crystallographic asymmetric unit. A noncrystallographic 3-fold relates the three subunits into a symmetric triad. Each subunit makes contact with the two others in the triad through interaction of catalytic and allosteric domains. Subunits are colored the same as in panel A. All protein structure figures were generated using the program Molscript (*47*) and rendered with Raster3D (*48*).

dimer interactions appear to provide the greatest stabilizing force between triads (Table 2).

The catalytic domain dimer is less substantial than the allosteric dimer (Figure 3B). Catalytic domain dimerization interactions are mediated mainly by packing of the helix formed by residues 172−188. These interactions are not the same as observed in the catalytic domain interface in the dimeric ATP sulfurylase from the bacterial *Riftia* symbiont (to be published).

Summing all of the interactions of the three types of domains reveals that in total, each subunit contacts four of the other five subunits within the hexamer. These connections not only stabilize the hexamer, but also provide a route by which a ligand-induced change in one subunit can be transmitted to every other subunit, a requirement of the concerted transition (symmetry) model of allosteric enzymes (*25*). A central cavity ranging from 15 Å wide in diameter at its entrance to 70 Å in the center of the hexamer runs along the 3-fold axis. The cavity may provide space to accommodate the movement of subunits during the allosteric transition.

Active Site. The APS molecule bound to the catalytic domain reveals the location of the active site. As shown in Figure 4A, the active site resides in a cavity contiguous with the bulk solution, and not with the central solvent channel. Figure 4B illustrates the specific interactions between bound APS and the enzyme. The sulfate moiety of APS is tethered

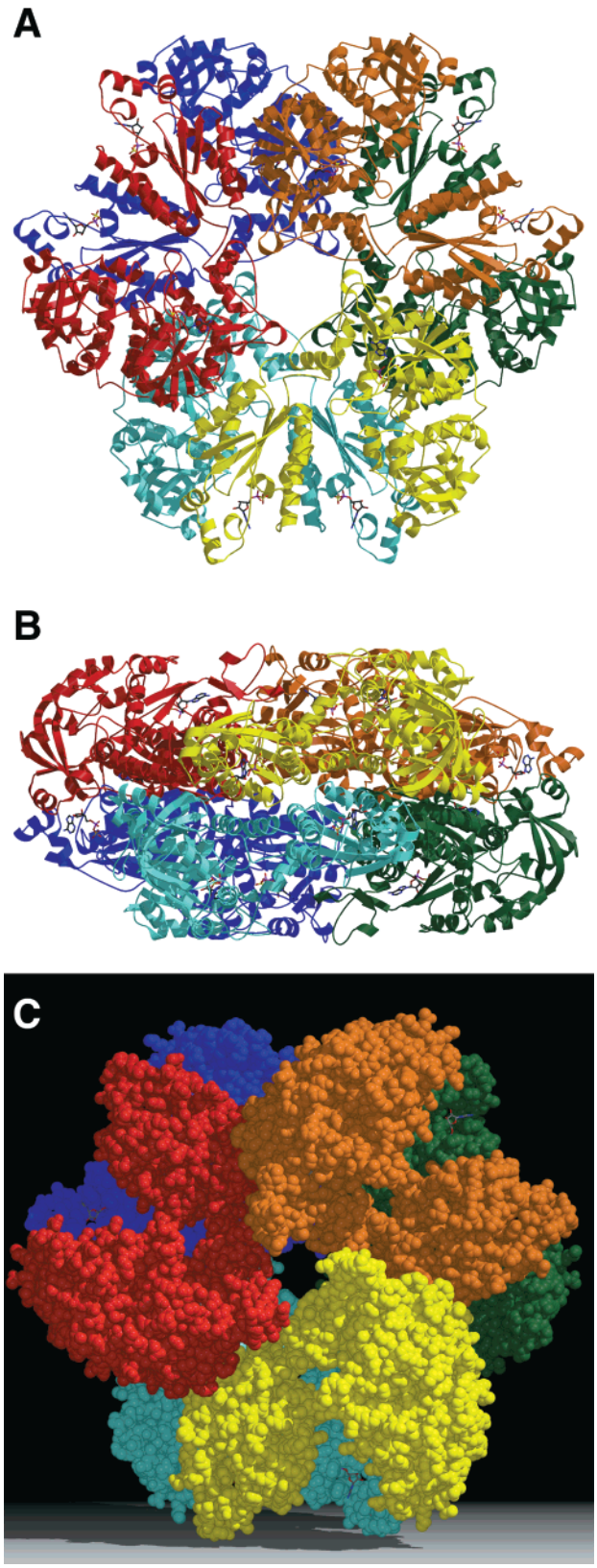

FIGURE 2: (A) Ribbon diagram of the ATP sulfurylase hexamer viewed along the noncrystallographic 3-fold. Each subunit is colored a single color for clarity. (B) Hexamer rotated 90° about the horizontal axis from diagram A. The enzyme is seen to be an oblate ellipsoid with dimensions of 140 Å × 70 Å. A 15−70 Å wide solvent-accessible channel exists along the 3-fold axis. (C) Space-filling model of the ATP sulfurylase hexamer viewed along the noncrystallographic 3-fold. Note that each subunit makes contact with four others. For example: red with both orange and yellow in the same triad and with blue and cyan in the other triad.

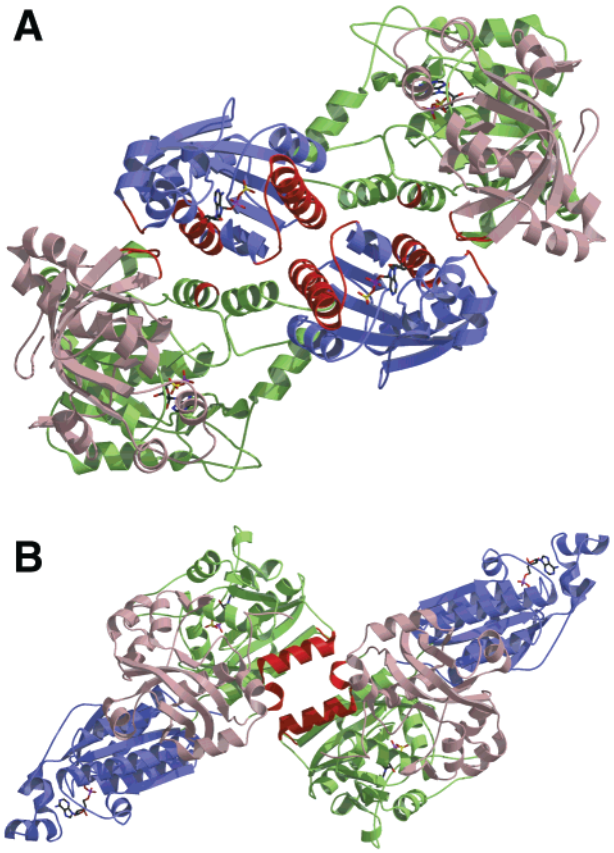

FIGURE 3: (A) Allosteric domain dimer. Allosteric domains (blue) of opposing triads dimerize across the crystal 2-fold. Domains are colored as in Figure 1 except for contact points between subunits, which are highlighted in red. (B) Catalytic domain dimer. Catalytic domains (green) also dimerize at the triad interface. Coloring is the same as in panel A.

Table 2: Buried Surface Areas[a]

location	interaction	area (Å^2)
within the same subunit	C−N	1804.7
within the same triad	A−C	517.4
across the triad interface	A−A′	803.3
	A−N′	469.4
	A−C′	238.6
	C−C′	336.9

[a] The buried surface area between two interacting domains were calculated as [(domain 1 surface area + domain 2 surface area) − combined surface area]/2. N refers to the N-terminal domain (residues 2−170). C, the catalytic domain (171−395), and A, the allosteric domain, (396−573). Domains indicated with a prime sign are in the "other" triad. For any given subunit in one triad, the A−A′, A−N′, and A−C′ interactions are with the one subunit in the opposite triad, but the C−C′ interaction is with a different subunit of the other triad.

by hydrogen bonds between the nonbridging oxygen atoms to the amide nitrogen of Gln 197, the Nη1 guanidino nitrogen of Arg 199, and the main chain amide of Ala 295. Two phosphate nonbridging oxygen atoms accept hydrogen bonds from the amide nitrogen of Gln 200 and the main chain amide of Arg 199. The bridging oxygen of the phosphosulfate group is in hydrogen bonding distance to the Nη1 guanidino nitrogen of Arg 199. These interactions define a four-residue motif, ^{197}QXRN^{200}, responsible for all but one of the bonds to the phosphosulfate moiety of APS. The hydroxyl of Thr 198 is also within hydrogen bonding distance from one of the phosphate nonbridging oxygens; however,

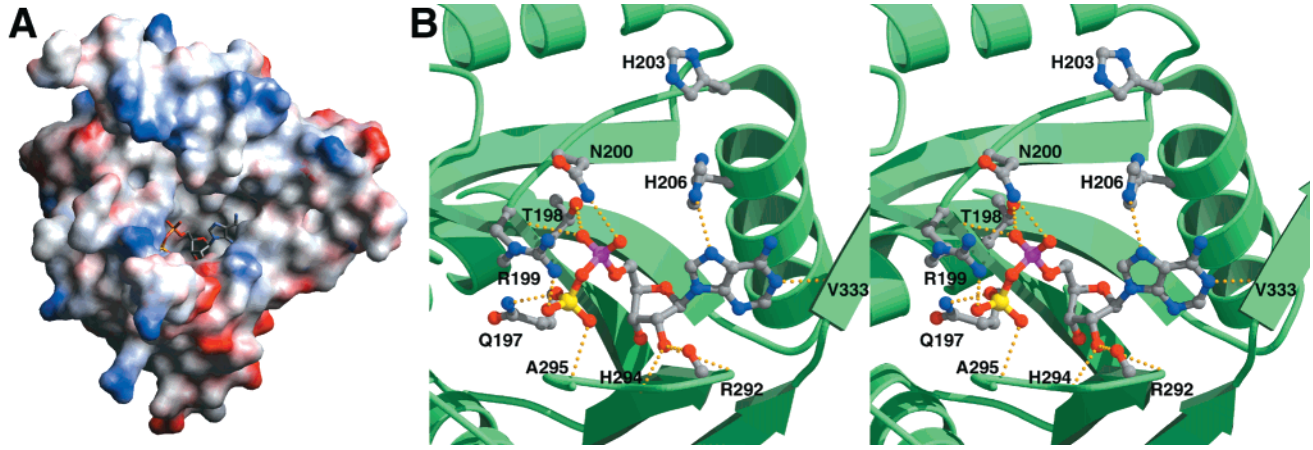

FIGURE 4: Two views of the catalytic domain showing bound APS. (A) Electrostatic surface diagram showing APS bound to the active site cavity. Surfaces are colored by electrostatic charge with positive and negative regions in blue and red, respectively. The cavity is accessible to substrates only from the external bulk solution. (B) Stereoview ribbon diagram showing residues that interact with bound substrates. Dashed gold lines represent potential hydrogen bonds.

this residue is not conserved in all ATP sulfurylases (*23*).

The motif ^{203}HXXH^{206} is a common feature of nucleotidyl transferases (*26*, *27*) and has been shown to be critical for catalysis in mammalian ATP sulfurylases (*23*, *24*). In our structure, the two His residues are positioned near the α-phosphoryl of APS, in position to bind $MgPP_i$ or the *β*- and *γ*-phosphates of ATP, as seen in crystals of the structurally related glutaminyl-tRNA synthetase (*22*). His 206 interacts with the N7 nitrogen of the adenine ring of APS through a weak hydrogen bond and thus, the binding of APS may help position this side chain. This idea is consistent with the observation that $MgPP_i$ will bind to the enzyme only in the presence of APS (*28*). The structural features of the catalytic site are consistent with earlier studies demonstrating the ability of active site ligands to protect against enzyme inactivation by reagents that covalently modify His or Arg side chains (*3*, *4*, *23*, *29*, *30*). Also, site-directed mutagenesis experiments have demonstrated that residues corresponding to Arg 199, His 203, and His 206, are essential for sulfurylase activity (*23*, *24*).

The sequence ^{288}FIVGRDHA^{295} may be part of a general adenylyl-binding motif which, if indicated as $(\text{hydrophobic})_{3-4}$-G-R/K-D-X-S/A, is also present in the *cys*-D subunit of heterooligomeric ATP sulfurylase from *E. coli* (*31*). *Cys*-D does not otherwise show strong homology to the homooligomeric ATP sulfurylases from fungi, etc. The motif appears to be part of a still larger structure ("PP loop") found in enzymes that catalyze the cleavage of ATP between the α and *β* phosphates (*23*, *32*).

ATP sulfurylase has been shown to have a strong preference for ATP as a substrate over other nucleoside triphosphates (*33*). The preference for adenine nucleotides can be explained by a hydrogen bond in which the N1 nitrogen of the adenine ring is the hydrogen acceptor and the main chain amide of Val 333 is the hydrogen donor. Pyrimidine nucleotides would be too far from the Val 333 main chain amid to make this hydrogen bond, and N1 nitrogen of guanine nucleotides is protonated and thus cannot be a hydrogen bond acceptor. The 2′-hydroxyl of the APS ribose is within hydrogen bonding distance from the main chain amide nitrogen of Arg 292, the main chain carbonyl oxygen of Arg 292, and the main chain amide nitrogen of His 294. These interactions account for the enzyme's preference for ATP over deoxy-ATP (*33*).

Allosteric Domain. Specific interactions between APS and the allosteric domain are shown in Figure 5. The phosphosulfate moiety of APS is bound to the enzyme in a bidentate salt linkage with the guanidino head of Arg 437. The adenine ring is held by *π*-orbital stacking between Phe 446 and Phe 529. Asp 434 hydrogen bonds to the 3′-hydroxyl of the ribose ring of APS. The presence of a phosphoryl group on the 3′-hydroxyl, as in the case of PAPS, would most likely displace Asp 434. All of these residues are strictly conserved in the sequence of APS kinase from fungi (*7*), plants (*34*), bacteria (*35*), and animals (*36*), indicating that the mode of APS binding observed in the allosteric domain of ATP sulfurylase is same as in true APS kinase

Figure 6 shows the superimposition of the polypeptide backbones of the APS kinase-like allosteric domain of *P. chrysogenum* ATP sulfurylase and the homologous APS kinase (*6*) from the same organism. The two structures superimpose very closely with an rms deviation of 1.69 Å for 140 equivalent C-α atoms. The only deviations seen are confined to allosteric domain residues 433−453 and residues 508−533. The 433−453 stretch contains Arg 437 and Phe 446 which directly contact the APS molecule bound to the allosteric domain (see Figure 5). The crystal structure of APS kinase was solved in the absence of any ligands, and therefore, the differences in this region may be attributed to the induced fit binding of APS. Figure 7 compares the sequences of true APS kinase and the allosteric domain of fungal ATP sulfurylase.

Allosteric domain residues 513−533 are analogous to the ATP "lid" in true APS kinase (residue stretch 149−169). In ligand-free APS kinase, this region is disordered and highly susceptible to cleavage by trypsin at Arg 158. Bound APS, PAPS, or MgATP protect APS kinase against proteolysis (*6*). The analogous region in *P. chrysogenum* ATP sulfurylase with APS bound at the allosteric site is highly ordered. Consistent with the correlation between orderliness of the lid region and susceptibility to trypsin, nucleotides protected ATP sulfurylase against tryptic cleavage at Lys 527 (*5*).

Surface Trench. The crystal structure revealed the presence of a surface trench linking each active site to an allosteric

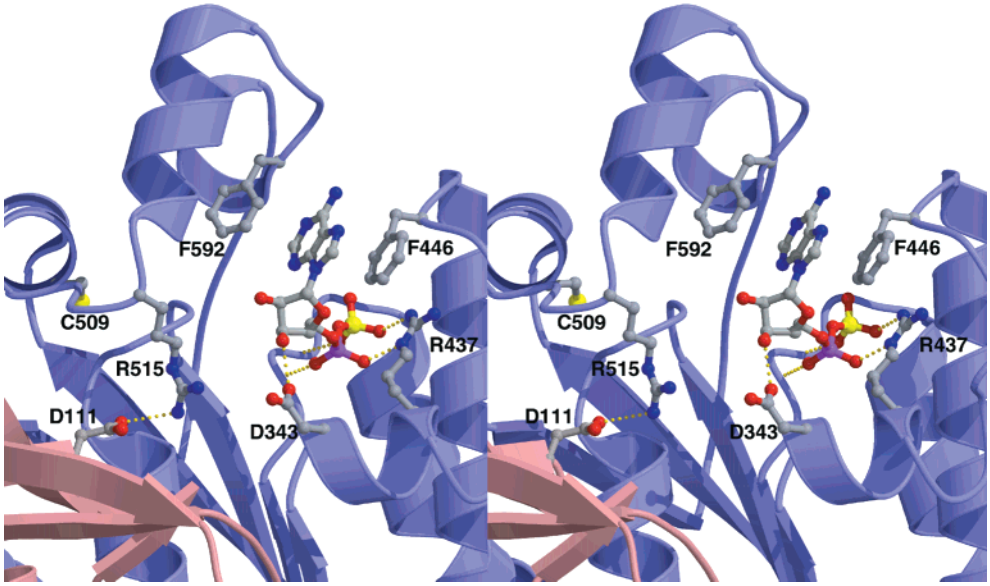

FIGURE 5: Allosteric site showing the bound APS molecule (stereo). Amino acids making specific contacts to APS are shown. Arg 515, which is well positioned to bind the 3′-hydroxyl of PAPS, is also shown in a salt linkage to Asp 111 of the N-terminal domain of an adjacent subunit. Gold dashed lines represent hydrogen bonds.

FIGURE 6: Superimposition of the ATP sulfurylase allosteric domain and APS kinase C-α backbones. The allosteric domain is shown in blue and APS kinase in yellow. The APS molecule bound in the allosteric domain structure is also shown interacting with allosteric domain residues Arg 437, Phe 446, and Phe 529.

site on a subunit of the opposing triad (Figure 8). The function of the trench is unknown. It could simply be a structural artifact of hexamer formation without any functional or evolutionary significance. Or the trench may be a vestigial feature of a bifunctional ("PAPS synthetase") ancestor of fungal ATP sulfurylase. If the latter is true, the evolutionary precursor might resemble the *Aquifex aeolicus* enzyme in which the APS kinase domain is C-terminal to the ATP sulfurylase region and presumably, is catalytically active. (The domains of the bifunctional enzyme from animal cells (*37*), which reportedly channels APS from one active site to the other (*38*, *39*), has the opposite order: APS kinase—ATP sulfurylase. The animal enzyme also appears to be a dimer.)

DISCUSSION

The X-ray structure of *P. chrysogenum* ATP sulfurylase, crystallized in the presence of a high concentration of APS, has been determined to 2.8 Å resolution. Each subunit of the homohexameric enzyme is composed of three structurally distinct globular regions. These are an N-terminal domain (residues 1−170), a central catalytic domain (residues 171−395), and a C-terminal allosteric domain (residues 396−573). The subunits are organized as a dimer of triads. Each subunit makes contact with four others—two in the same triad and two in the opposing triad. These interlocking linkages provide a means of transmitting a structural change in one subunit to all of the others, i.e., a way to propagate a concerted allosteric transition. The overall structure of fungal ATP sulfurylase is reminiscent of that of aspartate transcarbamoylase (*40*), except in fungal ATP sulfurylase, the allosteric and catalytic domains reside on the same polypeptide chain. [An aspartate transcarbamoylase in which the catalytic and regulatory peptides are fused into a single polypeptide has been described (*41*).]

The concerted transition model of allosteric enzymes requires that the protein be able to assume at least two distinct conformations. These are (a) the R state, which has the higher affinity for substrates and allosteric activators and a lower affinity for allosteric inhibitors and (b) the T state, which has the opposite ligand binding preferences. It was previously shown that the binding of APS to ATP sulfurylase dramatically stabilizes the R state even in the presence of PAPS (*1*). Consequently, we believe the presented structure to be the R state of the enzyme even though APS bound at both the catalytic and allosteric sites. This conclusion is supported by the observation that all three catalytic site APS molecules in the asymmetric unit had very well-defined electron density and an average *B*-factor of 52.3 Å^2 (the average Wilson plot *B*-factor was 75.0 Å^2 for all recorded data). APS molecules

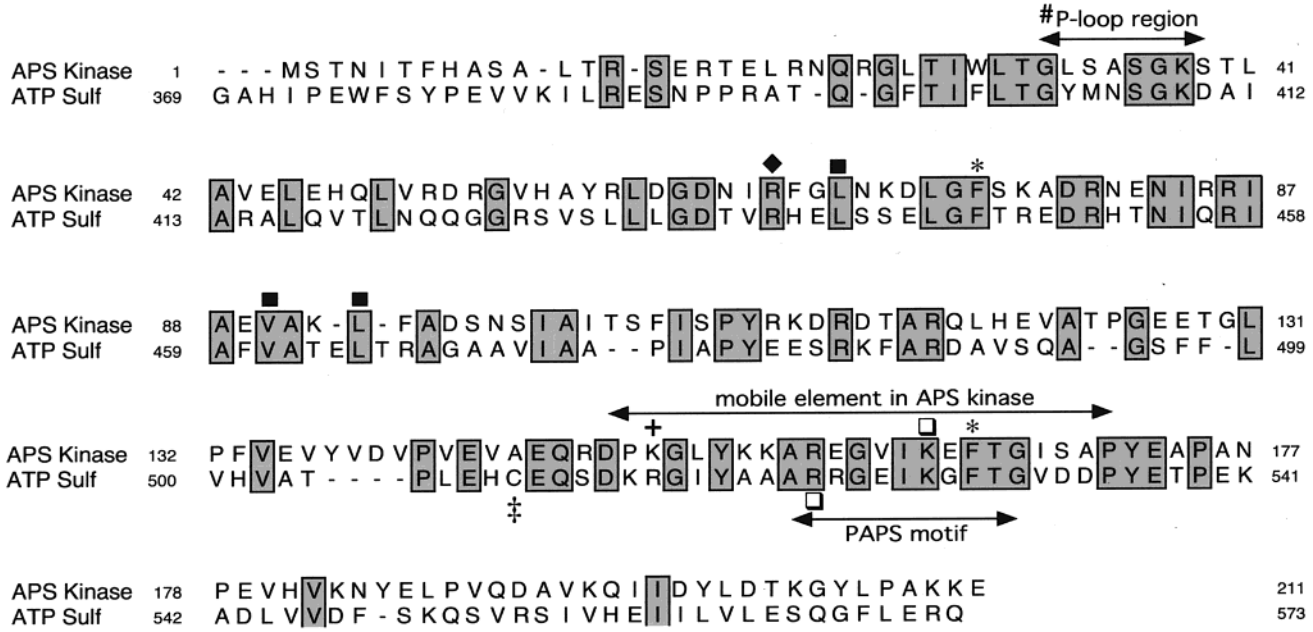

FIGURE 7: Sequence alignment of *P. chrysogenum* APS kinase and the C-terminal allosteric domain (residues 396−573) of ATP sulfurylase from this organism. The sequences are 44% identical in the core region (residues 396−539). Key residues and regions are indicated as follows: (#) P-loop region. ^{32}GLSASGKS^{39} of true APS kinase is altered to ^{403}GYMNSGKD^{410} in ATP sulfurylase. (■) Three hydrophobic residues present at the APS kinase dimer interface are conserved in the allosteric domain dimer interface in ATP sulfurylase. (*) Phe residues 75/446 and 165/529 straddle the adenine rings of bound nucleotide in ATP sulfurylase. (□) Both enzymes possess a "quick trypsin" site within the region corresponding to the mobile loop of true APSK. (◆) Arg 66/437 salt-links to the phosphosulfate group of bound APS in ATP Sulfurylase. (‡) Cys 509 is the residue that, if covalently modified or replaced by Ser or Tyr, induces positive cooperativity in the enzyme at pH 8, 30 °C in the absence of PAPS. (+) Lys 151/Arg 515 salt- links to the 3′-phosphate group of bound PAPS in ATP Sulfurylase.

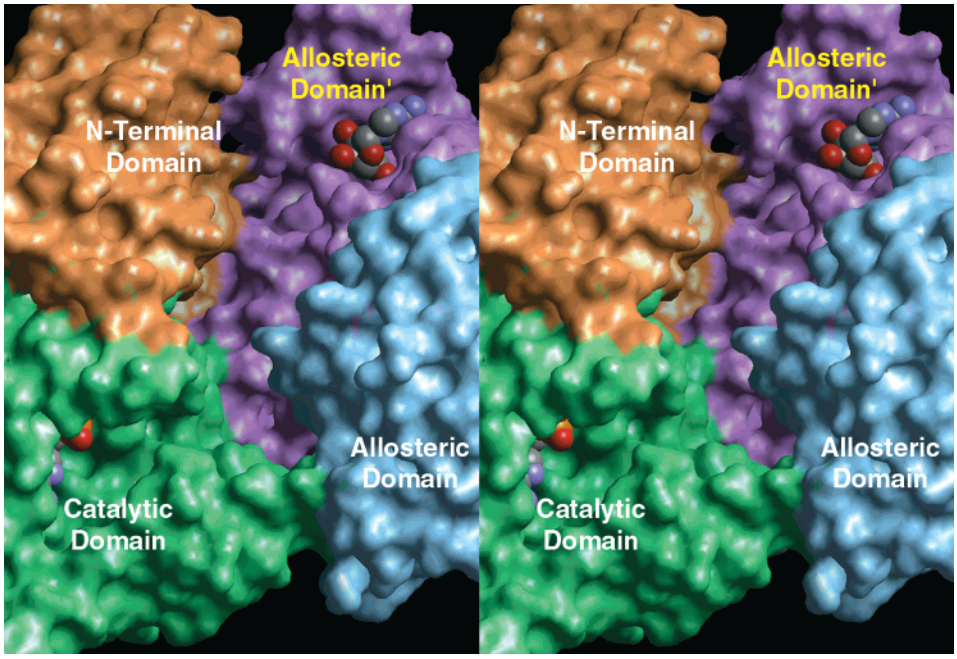

FIGURE 8: Surface diagram (stereoview) showing the "trench" linking the catalytic site of a subunit in one triad with the allosteric site of a symmetry related subunit in the opposite triad. APS molecules are shown in CPK space filling representation at each site. Domains are colored as in Figure 1 except for the symmetry related allosteric domain (allosteric domain′), which is purple.

at the allosteric site did not appear to be bound as tightly. The average *B*-factor for these molecules was 69.6 Å^2, and the corresponding electron density was interpretable, but not as well defined. It is possible that APS may compete with PAPS for the allosteric site, but not be able to induce the allosteric transition. This scenario might explain the two classes of APS binding sites observed in equilibrium binding studies (*4*). It is also possible that the binding of APS to the allosteric site may just be an artifact of the crystallization conditions. (It should be noted that this is not the first observation of APS interacting with a PAPS subsite (*42*).)

Although we cannot yet describe how the R and T states differ, the homology of the allosteric domain to true APS kinase suggests two specific structural changes that may contribute to the R−T transition. One such change is movement of residue stretch 513−533, a region that is

analogous to a mobile element or "lid" (residues 149−169) in true APS kinase (*6*). In kinases, this lid is believed to move and cover the active site after MgATP binds to the P-loop region (*43*). The kinase lid may also help to orient the phosphoryl acceptor. In fact, the analogous residue stretch in the allosteric domain of fungal ATP sulfurylase contains Phe 529, which together with Phe 446 straddle the adenine ring of the bound APS (Figure 6). While it is unlikely that the allosteric domain of ATP sulfurylase binds ATP [because of modifications to the P-loop and to an essential Asp (*7*)], there is evidence that the lid moves during the R−T transition. For example, covalent modification of Cys 509 (*4*) or replacement of this residue with Tyr or Ser induces sigmoidal kinetics (at pH 8, 30 °C) in the absence of PAPS (*5*). Also, the lid regions of ligand-free C509Y and C509S are more susceptible to cleavage by trypsin than that region in the ligand-free wild-type enzyme (*5*). These effects suggest that the modified enzymes exist mainly in the T state where the lid is in a more "open" conformation compared to that in the R state of the wild type enzyme. As shown in Figure 5, Cys 509 resides in a short helix immediately preceding the lid region. In the quaternary structure presented in this report (presumably, the R state), the lid makes contact with an N-terminal domain across the triad interface (Figure 5). Simultaneously, the side chain of Cys 509 packs tightly into a small hydrophobic pocket in the "hinge" region of the lid. Consequently, enlarging the side chain of Cys 509 by covalent modification with NEM or DTNB, or replacing the residue with an amino acid having a larger side chain would sterically hinder the insertion of the side chain into the hydrophobic pocket and thus, force the lid to remain in an "open" conformation. Replacement of Cys 509 with Ser would not sterically hinder lid closure to the R state conformation, but the less favorable interaction of the polar serine side chain with the hydrophobic pocket would have a similar effect on the T/R equilibrium. (In this regard, the crystal structures of C509Y and C509S should be informative.) In the wild-type enzyme, attraction of the Arg 515 side chain to the 3′-phosphate group of bound PAPS may unlink the lid from its interacting partner (Asp 111) in the opposing triad and thus, initiate the R to T transition. (The kinetic properties of R515 mutants would be informative.)

Subunit dissociation is another property of true APS kinase (*44*) that may have been recruited by ATP sulfurylase to serve as a basis of the R−T transition. While the partners of the trans-triad allosteric domain "dimer" may not be able to separate completely from each other, PAPS may trigger a movement of one partner relative to the other by diminishing the strength of certain interface bonds. Many of the interface residues of true APS kinase are also present in the allosteric domain of fungal ATP sulfurylase. Yet the allosteric domain dimer of ATP sulfurylase described in this report has a different interface orientation than that seen in true APS kinase. Thus, there is no doubt that there are at least two ways in which APS kinase (or APS kinase-like) subunits can associate. Perhaps one arrangement helps to stabilize the R state while the other arrangement might be favored in the T state.

Presumably, the allosteric domain of the fungal enzyme arose by APS kinase gene duplication, recombination, and independent evolution. The ancestral protein of the fungal ATP sulfurylase may have been a bifunctional PAPS synthetase (and the surface trench may be a vestige of an intersite substrate-channel). It is not surprising then that the sequence (or a variant of) ^{396}GFTIFLTG^{403}, which is present at the start of the allosteric domain of fungal ATP sulfurylase is also present in APS kinases. But interestingly, this motif is also present in yeast ATP sulfurylase as ^{395}GFSIVL-G^{401}, although the rest of the C-terminal region of this enzyme has little sequence homology to APS kinase or to the allosteric domain of the fungal enzyme. Perhaps yeast ATP sulfurylase is derived from the same bifunctional ancestor as the fungal enzyme, but its C-terminal domain was eventually modified until it no longer had APS kinase activity or sulfonucleotide binding properties.

Recently, the crystal structure of ATP sulfurylase from yeast was reported (*46*). While that enzyme does not exhibit allosteric properties, its multidomain features are very similar to those we report here. Unfortunately, a direct comparison between the fungal and yeast enzymes cannot be made at this time because the yeast coordinates are not yet available. However, the catalytic domains of the fungal and yeast enzymes have the same overall topology and the reported contacts made to APS by active site residues are nearly identical. Major differences between the two enzymes appear to be restricted to the C-terminal domains where sequence similarity is very low. While the C-terminal domains of the two enzymes have similar overall topologies, there are multiple deletions of loops and other secondary structural elements in the yeast enzyme that are important for PAPS binding in the fungal enzyme. Finally, several cadmium ions were observed in the structure of the yeast enzyme, but no divalent cations were seen in the present *P. chrysogenum* structure.

The results presented in this report are just a beginning of our understanding of the structure−function relationships of a homooligomeric enzyme that: (a) runs the native aggregate gamut from dimer (e.g., the bacterial *Riftia* symbiont or animal enzyme) (*29*, *30*) through tetramer (e.g., the plant enzyme) (*45*), and hexamer (e.g., the fungal and yeast enzymes). (b) Exists as a monofunctional enzyme in some organisms (e.g., fungi, yeasts, plants, some bacteria) and in a bifunctional form in others (e.g., animal sources). (c) Exists in both allosteric and nonallosteric forms. (d) Is optimized for APS synthesis in sulfate assimilators, but for the ATP synthesis direction in chemolithotrophs (*29*).

ACKNOWLEDGMENT

Some of the work reported here was performed at SRRL, which is operated by the Department of Energy, Office of Basic Energy Sciences. The SSRL Biotechnology Program is supported by the National Institutes of Health, National Center for Research Resources, Biomedical Technology Program, and by the Department of Energy, Office of Biological and Environmental Research.

REFERENCES

1. MacRae, I., and Segel, I. H. (1997) *Arch. Biochem. Biophys. 337*, 17−26.
2. Renosto, F., Martin, R. L., Wailes, L. M., Daley, L. A., and Segel, I. H. (1990) *J. Biol. Chem. 265*, 10300−10308.
3. Foster, B. A., Thomas, S. M., Mahr, J. A., Renosto, F., Patel, H., and Segel, I. H. (1994) *J. Biol. Chem. 269*, 19777−19786.

4. Renosto, F., Martin, R. L., and Segel, I. H. (1987) *J. Biol. Chem. 262*, 16279−16288.
5. MacRae, I. J., Hanna, E., Ho, J. D., Fisher, A. J., and Segel, I. H. (2000) *J. Biol. Chem. 275*, 36303−36310.
6. MacRae, I. J., Segel, I. H., and Fisher, A. J. (2000) *Biochemistry 39*, 1613−1621.
7. MacRae, I., Rose, A. B., and Segel, I. H. (1998) *J. Biol. Chem. 273*, 28583−28589.
8. Segel, I. H., Renosto, F., and Seubert, P. A. (1987) in *Methods in Enzymology* (Jakoby, W. B., and Griffith, O. W., Eds.) pp 334−349, Academic Press, San Diego.
9. Otwinowski, Z., and Minor, W. (1997) in *Methods in Enzymology* (C. W. Carter, J., and Sweet, R. M., Eds.) pp 307−326, Academic Press, New York.
10. Furey, W., and Swaminathan, S. (1997) *Methods Enzymol. 277*, 590−620.
11. Terwilliger, T. C., and Berendzen, J. (1999) *Acta Crystallogr., Sect. D 55*, 849−861.
12. Terwilliger, T. C. (2000) *Acta Crystallogr., Sect. D 56*, 965−972.
13. Terwilliger, T. C. (1999) *Acta Crystallogr., Sect. D 55*, 1863−1871.
14. CCP4. (1994) *Acta Crystallogr., Sect. D 50*, 760−763.
15. Jones, T. A., Zou, J. Y., Cowan, S. W., and Kjeldgaard, M. (1991) *Acta Crystallogr., Sect. A 47*, 110−119.
16. Brünger, A. T., Adams, P. D., Clore, G. M., DeLano, W. L., Gros, P., Grosse-Kunstleve, R. W., Jiang, J.-S., Kuszewski, J., Nilges, M., Pannu, N. S., Read, R. J., Rice, L. M., Simonson, T., and Warren, G. L. (1998) *Acta Crystallogr., Sect. D 54*, 905−921.
17. Brünger, A. T. (1993) *Acta Crystallogr., Sect. D 49*, 24−36.
18. Laskowski, R. A., MacArthur, M. W., Moss, D. S., and Thornton, J. M. (1993) *J. Appl. Crystallogr. 26*, 283−291.
19. Holm, L., and Sander, C. (1993) *J. Mol. Biol. 233*, 123−138.
20. Rossmann, M. G., Moras, D., and Olsen, K. W. (1974) *Nature 250*, 194−199.
21. Izard, T., and Geerlof, A. (1999) *EMBO J. 18*, 2021−2030.
22. Rould, M. A., Perona, J. J., and Steitz, T. A. (1991) *Nature 352*, 213−218.
23. Deyrup, A. T., Singh, B., Krishnan, S., Lyle, S., and Schwartz, N. B. (1999) *J. Biol. Chem. 274*, 28929−28936.
24. Venkatachalam, K. V., Fuda, H., Koonin, E. V., and Strott, C. A. (1999) *J. Biol. Chem. 274*, 2601−2604.
25. Monod, J., Wyman, J., and Changeux, J.-P. (1965) *J. Mol. Biol. 12*, 88−118.
26. Bork, P., Holm, L., Koonin, E. V., and Sander, C. (1995) *Proteins: Struct., Funct., Genet. 22*, 259−266.
27. Veitch, D. P., and Cornell, R. B. (1996) *Biochemistry 35*, 10743−10750.
28. Seubert, P. A., Hoang, L., Renosto, F., and Segel, I. H. (1983) *Arch. Biochem. Biophys. 225*, 679−691.
29. Renosto, F., Martin, R. L., Borrell, J. L., Nelson, D. C., and Segel, I. H. (1991) *Arch. Biochem. Biophys. 290*, 66−78.
30. Yu, M., Martin, R. L., Jain, S., Chen, L. J., and Segel, I. H. (1989) *Arch. Biochem. Biophys. 269*, 156−174.
31. Leyh, T., Vogt, T. F., and Suo, Y. (1992) *J. Biol. Chem. 267*, 10405−10410.
32. Bork, P., and Koonin, E. V. (1994) *Proteins: Struct., Funct., Genet. 20*, 347−355.
33. Tweedie, J. W., and Segel, I. H. (1971) *Prepr. Biochem. 1*, 91−117.
34. Arz, H. E., Gisselmann, G., Schiffmann, S., and D., S. J. (1994) *Biochim. Biophys. Acta 1218*, 447−452.
35. Leyh, T. S., Taylor, J. C., and Markham, G. D. (1988) *J. Biol. Chem. 263*, 2409−2416.
36. Li, H., Deyrup, A., Mensch, J. R. J., Domowicz, M., Konstantinidis, A. K., and Schwartz, N. B. (1995) *J. Biol. Chem. 270*, 29453−29459.
37. Lyle, S., Stanczak, J., Ng, K., and Schwartz, N. B. (1994) *Biochem. 33*, 5920−5925.
38. Lyle, S., Ozeran, J. D., Stanczak, J., Westley, J., and Schwartz, N. B. (1994) *Biochemistry 33*, 6822−6827.
39. Lyle, S., Stanczak, J. D., Westley, J., and Schwartz, N. B. (1995) *Biochemistry 34*, 940−945.
40. Monaco, H. L., Crawford, J. L., and Lipscomb, W. N. (1978) *Proc. Natl. Acad. Sci. U.S.A. 75*, 5276.
41. Chen, P., Van Vliet, F., Van De Casteele, M., Legrain, C., Cunin, R., and Glansdorff, N. (1998) *J. Bacteriol. 180*, 6389−6391.
42. MacRae, I. J., and Segel, I. H. (1999) *Arch. Biochem. Biophys. 361*, 277−282.
43. Schlauderer, G. J., Proba, K., and Schulz, G. E. (1996) *J. Mol. Biol. 256*, 223−227.
44. Renosto, F., Seubert, P. A., Knudson, P., and Segel, I. H. (1985) *J. Biol. Chem. 260*, 1535−1544.
45. Renosto, F., Patel, H. C., Martin, R. L., Thomassian, C., Zimmerman, G., and Segel, I. H. (1993) *Arch. Biochem. Biophys. 307*, 272−285.
46. Ullrich, T. C., Blaesse, M., and Huber, R. (2001) *EMBO J. 20*, 316−329.
47. Kraulis, P. J. (1991) *Journal of Applied Crystallography 24*, 946−950.
48. Merritt, E. A., and Murphy, M. E. P. (1994) *Acta Crystallogr. 50*, 869−873.

BI010367W